Journal of Intelligent & Robotic Systems (2020) 99:129–145
https://doi.org/10.1007/s10846-019-01102-1

A Full Hydrodynamic Consideration in Control System Performance Analysis for an Autonomous Underwater Vehicle

Mojtaba Mirzaei [1] · Hossein Taghvaei [2]

Received: 14 February 2019 / Accepted: 13 September 2019 / Published online: 7 November 2019

Abstract
Autonomous underwater vehicles (AUVs) have important applications in several areas such as data collection, geological survey and exploration in underwater environment. The hydrodynamic forces acting on AUVs are highly nonlinear and the higher-order hydrodynamic coefficients should be taken into account to represent these nonlinear behaviors. Therefore, developing a suitable dynamic model of the AUV and also an accurate knowledge about the hydrodynamic parameters are important for proper design of the navigation and control system. The main goal of the present paper is to investigate the role of proper dynamic model for an AUV which includes different hydrodynamic stability derivatives coefficients. Design of proper actuator is also significant for the global performance of the system and the expenses of the plan. It is tried in the present paper to investigate the effect of full hydrodynamic coefficients on the design of actuators and control system performance analysis for an AUV which was ignored in the previous works. For this purpose, the effect of these parameters on the open loop characteristics of the AUV, its role in the control system design and the interaction of control system and actuator dynamics are considered in nonlinear time domain and frequency domain. It is shown that in a full hydrodynamic consideration for design of the AUV, the effect of control gains, system bandwidth and damping can be different in comparison with the cases which are not fully considered them. Finally, the design of optimum actuator and the effect of actuator natural frequency on the flight performance in the presence of full hydrodynamic coefficients are studied.

Keywords Full hydrodynamic consideration · System bandwidth · Actuator design · Control system performance analysis · Autonomous underwater vehicle

1 Introduction

Autonomous underwater vehicles (AUVs) have been used for a variety of tasks including data collection, geological survey and exploration in underwater environment [1]. The hydrodynamic forces acting on an underwater vehicle are highly nonlinear and the mathematical models should take into account higher-order hydrodynamic coefficients to represent these nonlinear behaviours [2, 3]. There is always a need for suitable dynamic model of the vehicle and also an accurate knowledge about the hydrodynamic parameters in order to successful design of the navigation and control system for an AUV [4]. The main goal of this article is the investigation of the role of proper dynamic model for an AUV which is of great importance in terms of designing the control and guidance system. Some researchers argued that the greatest problem in designing a suitable controller for AUVs is knowing the values of hydrodynamic parameters with sufficient accuracy [5]. Different methods are used to determine the hydrodynamic parameters, including experimental studies, computational fluid dynamics (CFD), and the use of fast computational codes such as Datcom. One of the commonly used experimental methods for measuring hydrodynamic stability derivatives coefficients is the decay test, first proposed by Morrison [6], but experimental methods for calculating hydrodynamic coefficients such as water tunnel or water channel usually require considerable cost and time [7, 8]. Eng et al. [9] used an experimental method to calculate hydrodynamic forces for a submarine robot. The method used by them is based on the conventional decay test, but with difference that the spring oscillations are replaced by the movement of a pendulum. Nowadays, computational fluid dynamic based methods have been taken into consideration by many researchers in order to

✉ Mojtaba Mirzaei
mmirzaei@shirazu.ac.ir

[1] Hydro-Aeronautical Research Center, Shiraz University, Shiraz, Iran

[2] School of Mechanical Engineering, Shiraz University, Shiraz, Iran

calculate the hydrodynamic forces on an AUV. Suzuki et al. [10], for example, calculated the hydrodynamic and added mass coefficients for an underwater vehicle and validated the results of numerical calculations with experimental results. The studies carried out by them indicate that the results of CFD have an acceptable matching with experimental results. Also, Praveen and Krishnankutty [11] used CFD method and conducted water channel experiments to investigate the effect of the length of an underwater vehicle on hydrodynamic forces and showed that the linear coefficients changes linearly with the length; however the changes of nonlinear coefficients with the length showed to be nonlinear in the considered range. In addition to the above researches, online identification can be used to find the stability derivatives coefficients. Hong et al. [12] developed a technique to enable rapid identification of autonomous underwater robot dynamics online. They also showed that a gain-scheduled controller with better performance than a constant gain controller can be designed using online estimated parameters.

The hydrodynamic coefficients can be classified into static and dynamic stability derivatives coefficients. From past to the recent years, the interaction of control system and actuator dynamics has been focused for flying of AUVs. Static stability derivatives coefficients effects have been usually investigated for this purpose. Nesline et al. [13] studied the robustness of a tail controlled homing missile with constant gain autopilot with respect to variation of the static aerodynamic stability derivatives. The effect of the open loop crossover frequency and the actuator bandwidth on the allowable region of some of static stability derivatives coefficients for both a constant gain and available gain flight control system was also discussed. Chwa et al. [14] studied the effect of actuator dynamics on nonlinear missile control system. They showed that the first-order actuator dynamics has no influence on the reduction of q-dynamics via singular perturbation, but the second-order actuator may destabilize the q-dynamics. Also, they developed a compensator using the back-stepping technique in order to reduce the effect of actuator dynamics.

Fang et al. [15] presented a design for a two-loop acceleration autopilot of a tactical missile and introduced the equivalent actuator dynamics to obtain the overall stability condition. They showed that the autopilot control capacity is dominated by the actuator bandwidth. Li and Su [16] studied the nonlinear control of an autonomous underwater vehicle with internal actuators (internal moving mass) instead of control surfaces. They showed that the displacement of the internal mass in the sway direction can affect the flow of the dynamical system in phase space. They also designed a LQR controller to stabilize the heading angle of the vehicle.

Sun et al. [17] studied the PID pitch attitude control of an unstable flight vehicle in the presence of actuator delay. The effects of the integral action on the robustness and dynamic performance were investigated and the results showed that the moderate integral gain is appropriate to improve the dynamic performance. Wu et al. [18] designed an adaptive control architecture with anti-windup compensator for pitch channel control of a REMUS autonomous underwater vehicle with input saturation and coupling disturbances. They showed that the designed controller can tackle input saturation and can adapt to model uncertainties, coupling disturbances and noise.

Indiveri and Malerba [19] studied the complementary filtering for underwater robots with actuator redundancy. The proposed underwater vehicle had two actuation systems namely a ballast tank (which can be filled or emptied changing the restoring force acting on the vehicle) and a set of vertical jet thrusters (generating a vertical force). They also designed a PID controller implemented through an anti-windup architecture for vertical force to be generated to follow a depth profile.

Lea et al. [20] compared three control techniques namely the classical control, the fuzzy logic control and the sliding mode control for underwater robots. They showed that the classical control was the most simple, but required a basic system model for its design. The fuzzy logic controller was generated without a model, but required extensive tuning and the sliding mode controller was the most complex and required a complete system model. Hsu and Liu [21] studied the modification of control loop in order to improve the depth response of autonomous underwater robots. Two methods of modification of control loop are used to eliminate the steady-state depth errors. In the first method, the mean steady-state depth error which is an offset from the depth command is deducted. The second method which uses a switching integrator acts only when the depth error is below a certain threshold. Fossen [22] studied the guidance, navigation and control of ships and underwater vehicles. The PID control and acceleration feedback were considered and different case studies such as the heading autopilot, heading autopilot with acceleration feedback, linear cross-tracking system, LOS path-following using Serret-Frenet coordinates and dynamic positioning control system were presented, but the effect of dynamic stability derivatives coefficients is not considered for designing actuators.

The main goal of the present study is to investigate the effect of dynamic stability derivatives coefficients on the performance of an AUV, which will be finally used in the actuator design for different control channels and control system performance analysis. These coefficients are often not modeled in transformation functions and their effect is not investigated completely. Therefore, the effect of dynamic stability derivatives coefficients on natural frequency, damping coefficient and bandwidth for an AUV is investigated in order to design suitable actuators and control system in the present paper.

The rest of the paper is organized as follows: Section 2 studies the mathematical model for an AUV which represents the equations of motion and the calculation of hydrodynamic stability derivatives coefficients. The design of control system

for the AUV is presented in Section 3 and finally the simulation results are presented and discussed in Section 4.

2 Mathematical Modeling of the AUV

The equations of motion for an AUV are usually determined in body coordinate system or relative to a fixed or inertial coordinate system which are depicted in Fig. 1. As Fig. 1 shows, the notations x, y and z are the translational positions of the vehicle relative to the inertial coordinate system and φ, θ and ψ are the rotational positions of the vehicle relative to the inertial coordinate system. Also, u, v and w are the linear surge, sway and heave components of velocity in the body coordinate system respectively and p, q and r represent the components of angular velocity. The resultant forces exerted to the vehicle in the body coordinate system are represented by X, Y and Z and the resultant moments are expressed as: K, M and N in the body fixed coordinate system.

In the six-DOF model, the forces and moments that act on the rigid body include the hydrostatic force F_{HS} and moment M_{HS}, the lift F_{lift} and drag F_{drag} forces and their moments and the control inputs $F_{control}$ realized through the fins commands and their moments. The complete equations of motion for an AUV in the body fixed coordinate system can be represented as the following equations: [23, 24]:

$$m\left[\dot{u}-vr+wq-x_g\left(q^2+r^2\right)+y_g\left(pq-\dot{r}\right)+z_g\left(pr+\dot{q}\right)\right]=F_X \quad (1)$$

$$m\left[\dot{v}-wp+ur-y_g\left(r^2+p^2\right)+z_g\left(qr-\dot{p}\right)+x_g\left(qp+\dot{r}\right)\right]=F_Y \quad (2)$$

$$m\left[\dot{w}-uq+vp-z_g\left(p^2+q^2\right)+x_g\left(rp-\dot{q}\right)+y_g\left(rq+\dot{p}\right)\right]=F_Z \quad (3)$$

$$I_{xx}\dot{p}+\left(I_{zz}-I_{yy}\right)qr+m\left[y_g\left(\dot{w}-uq+vp\right)-z_g\left(\dot{v}-wp+ur\right)\right]=M_X \quad (4)$$

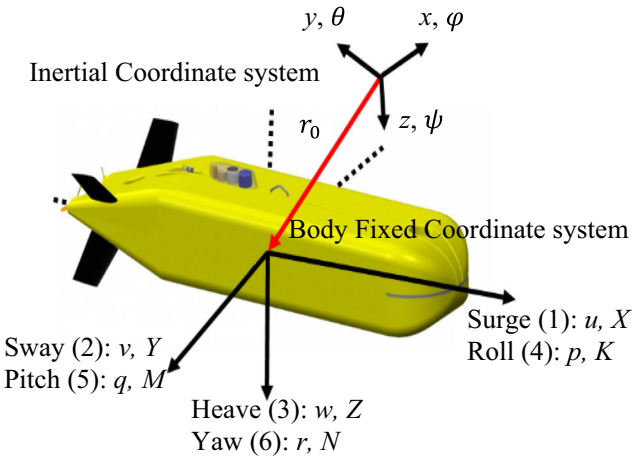

Fig. 1 Body and inertial coordinate systems for the AUV

$$I_{yy}\dot{q}+\left(I_{xx}-I_{zz}\right)rp+m\left[z_g\left(\dot{u}-vr+wq\right)-x_g\left(\dot{w}-uq+vp\right)\right]=M_Y \quad (5)$$

$$I_{zz}\dot{r}+\left(I_{yy}-I_{xx}\right)pq+m\left[x_g\left(\dot{v}-wp+ur\right)-y_g\left(\dot{u}-vr+wq\right)\right]=M_Z \quad (6)$$

In the above equations, m is the mass of the vehicle and x_g, y_g and z_g are locations of the center of mass of the vehicle in the body coordinate system. F_X, F_Y and F_Z are the external forces and M_X, M_Y and M_Z are the external moments in X, Y and Z directions respectively. The time derivatives of velocities in the surge, sway and heave directions are denoted by $\dot{u}$, $\dot{v}$ and $\dot{w}$ and the time derivatives of angular velocities for these directions are $\dot{p}$, $\dot{q}$ and $\dot{r}$ respectively. It should be noted that above equations are written assuming that the products of inertia are small, which means that the inertia matrix has only the diagonal elements I_{xx}, I_{yy} and I_{zz}.

The weight (W) and buoyancy (B) vectors in the inertial coordinate system can be represented as:

$$\vec{F}_W=\begin{bmatrix}0\\0\\mg\end{bmatrix}=\begin{bmatrix}0\\0\\W\end{bmatrix} \quad (7)$$

$$\vec{F}_B=\begin{bmatrix}0\\0\\-\rho\forall g\end{bmatrix}=\begin{bmatrix}0\\0\\-B\end{bmatrix} \quad (8)$$

where ρ is the density of water and $\forall$ is the total volume of the vehicle. Therefore, the vectors of hydrostatic force ($\vec{F}_{HS}$) and hydrostatic moment ($\vec{M}_{HS}$) in the body fixed coordinate system can be expressed as follows:

$$\vec{F}_{HS}=\hat{C}_{B-I}\times\vec{F}_W+\hat{C}_{B-I}\times\vec{F}_B \quad (9)$$

$$\vec{M}_{HS}=\vec{r}_g\times\left(\hat{C}_{B-I}\times\vec{F}_W\right)+\vec{r}_b\times\left(\hat{C}_{B-I}\times\vec{F}_B\right) \quad (10)$$

In the above equations, $\vec{r}_g$ and $\vec{r}_b$ are the position vectors of the center of gravity and the center of buoyancy in the body coordinate system and $\hat{C}_{B-I}$ is the transformation matrix from the body coordinate system to the inertial coordinate system which are represented as follows:

$$\vec{r}_g=\begin{bmatrix}x_g\\y_g\\z_g\end{bmatrix} \quad (11)$$

$$\vec{r}_b=\begin{bmatrix}x_b\\y_b\\z_b\end{bmatrix} \quad (12)$$

$$\hat{C}_{B-I} = \begin{bmatrix} cos\psi\ cos\theta & sin\psi\ cos\theta & -sin\theta \\ cos\psi\ sin\theta\ sin\varphi - sin\psi\ cos\varphi & sin\psi\ sin\theta\ sin\varphi + cos\psi\ cos\varphi & cos\theta\ sin\varphi \\ cos\psi\ sin\theta\ cos\varphi + sin\psi\ sin\varphi & sin\psi\ sin\theta\ cos\varphi - cos\psi\ sin\varphi & cos\theta\ cos\varphi \end{bmatrix} \tag{13}$$

The hydrodynamic forces and moments coefficients related to the drag, lift and control surfaces forces and moments can be represented as follows:

$$C_{F_X} = \frac{F_X}{0.5\rho V^2 A} = C_{X0} + C_{X\alpha^2}\alpha^2 + C_{X\beta^2}\beta^2 + C_{X\delta_e}|\delta_e| + C_{X\delta_e}|\delta_r| + C_{X\delta_a}|\delta_a| \tag{14}$$

$$C_{F_Y} = \frac{F_Y}{0.5\rho V^2 A} = C_{Y\beta}\beta + C_{Y\delta_r}\delta_r + C_{Yr}r + C_{Y\dot{\beta}}\dot{\beta} \tag{15}$$

$$C_{F_Z} = \frac{F_Z}{0.5\rho V^2 A} = C_{Z\alpha}\alpha + C_{Z\delta_e}\delta_e + C_{Zq}q + C_{Z\dot{\alpha}}\dot{\alpha} \tag{16}$$

$$C_{M_X} = \frac{M_X}{0.5\rho V^2 AD} = C_{K\delta_a}\delta_a + C_{Kp}p \tag{17}$$

$$C_{M_Y} = \frac{M_Y}{0.5\rho V^2 AD} = C_{M\alpha}\alpha + C_{M\delta_e}\delta_e + C_{Mq}q + C_{M\dot{\alpha}}\dot{\alpha} \tag{18}$$

$$C_{M_Z} = \frac{M_Z}{0.5\rho V^2 AD} = C_{N\beta}\beta + C_{N\delta_r}\delta_r + C_{Nr}r + C_{N\dot{\beta}}\dot{\beta} \tag{19}$$

In the above equations, C_{F_X}, C_{F_Y} and C_{F_Z} are the non-dimensional force coefficients and C_{M_X}, C_{M_Y} and C_{M_Z} are the non-dimensional moment coefficients for X, $Y$and Z directions respectively. The velocity magnitude of the vehicle is denoted by $V$and A is the reference area equal to $\pi D^2/4$, where, D is the diameter of the vehicle. Also, α and β indicate the angle of attack and side slip angle respectively and $\dot{\alpha}$ and $\dot{\beta}$ are time derivatives of angle of attack and side slip angle respectively. δ_a, δ_e and δ_r indicate the aileron, elevator and rudder control surface angles respectively. The subscripts of presented coefficients mean the differentiation about the parameter in the subscript. For example, $C_{X\delta_e}$ indicates the stability derivatives coefficient of force in x direction relative to the elevator control surface angle δ_e. Also, the subscript 0 in Eq. (14) represents the zero angle of attack, side slip angle and fin deflection angle. The force and moment coefficients used in the modeling are defined in Table 2.

The coefficients $C_{Z\dot{\alpha}}$, $C_{M\dot{\alpha}}$, C_{Zq}, C_{Mq}, $C_{Y\dot{\beta}}$, $C_{N\dot{\beta}}$, C_{Yr}, C_{Nr} and C_{Kp} are dynamic stability derivatives coefficients and the remaining coefficients are static stability derivatives coefficients. Dynamic stability derivatives coefficients are determined by differentiation of forces and moments relative to the angular velocities (p, q and r) or time derivatives of angle of attack and side angle ($\dot{\alpha}$ and $\dot{\beta}$). However, the static stability derivatives coefficients are determined by differentiation of forces and moments relative to the control surfaces angles (δ_a, δ_e *and* δ_r) or relative to the angle of attack and side angle (α and β). The coefficients $C_{Z\dot{\alpha}}$, $C_{M\dot{\alpha}}$, C_{Zq},$C_{Mq}$are related to the pitch and the coefficients $C_{Y\dot{\beta}}$, $C_{N\dot{\beta}}$, C_{Yr} and C_{Nr} are related to the yaw of the vehicle. It should be noted that, in the present research, the dynamic stability derivatives coefficients in roll direction are not considered and the focus is on the investigation of the dynamic stability effects on the yaw channel. In addition, according to the fact that the mentioned AUV has no considerable accelerating motion, the effect of added mass coefficients are not significant in the control system performance analysis which will be shown in the following section. The main geometric and inertia parameters of the considered AUV are presented in Table 1.

The considered AUV has four identical control fins which have a NACA 0012 cross-section and mounted in a cross pattern near the aft end of the hull.

As mentioned earlier, in order to investigate the effects of dynamic stability derivatives coefficients on the performance of the AUV and also on the design of proper actuators for the vehicle, the dynamic coefficients are firstly neglected and then they have been considered in simulations and the results of these two cases are compared with each other in order to select the proper actuator for the AUV. Datcom computational code is used for determination of static and dynamic stability derivatives coefficients which are presented in Table 2. Watson [25] studied the usability of DATCOM for the prediction of hydrodynamic loads on finned sections of missiles in incompressible flow and the results indicated that DATCOM may be applicable to incompressible flow problems.

3 Control System Analysis

The dynamics of the system has been determined in the previous sections and now the dynamics, controller and actuators can be combined in this section. Although there are various types of control algorithm, as previously described in introduction, such as fuzzy, nonlinear, adaptive and robust methods to control the AUVs [26]; the emphases in this paper is on the investigation of the effect of dynamic stability derivatives coefficients on the control system and actuator dynamic characteristics. Therefore, a classic PID controller with experimental considerations is implemented to achieve the aim of this

Table 1 Main geometric and inertia parameters of the AUV

Parameter	Value	Unit	Description
L	1.15	m	Vehicle total length
D	0.20	m	Maximum hull diameter
m	35	kg	Mass of vehicle
$\boldsymbol{I_{xx}}$	0.17	Kgm^2	Moment of inertia about the x axis
$\boldsymbol{I_{yy}}$	3.84	Kgm^2	Moment of inertia about the y axis
$\boldsymbol{I_{zz}}$	3.84	Kgm^2	Moment of inertia about the z axis
$\boldsymbol{b_{fin}}$	0.036	m	Span of control fins
$\boldsymbol{S_{fin}}$	4.44×10^{-4}	m^2	Area of control fins

Table 2 Hydrodynamic coefficients calculated by Datcom

Coefficient	Definition	Calculated value
C_{X0}	x force coefficient at zero angle of attack, side slip angle and fin deflection angle	−0.230
$C_{X\alpha^2}$	x force coefficient due to square of angle of attack variation	0.00013
$C_{X\beta^2}$	x force coefficient due to square of side slip angle variation	0.00013
$C_{X\delta_e}$	x force coefficient due to elevator angle variation	−0.00034
$C_{X\delta_a}$	x force coefficient due to aileron angle variation	−0.0007
$C_{Z\alpha} = C_{Y\beta}$	z force coefficient due to angle of attack variation = y force coefficient due to side slip angle variation	−0.0314
$C_{Z\delta_e} = C_{Y\delta_r}$	z force coefficient due to elevator angle variation = y force coefficient derivative with rudder angle variation	−0.008
$C_{Zq} = -C_{Yr}$	z force coefficient due to pitch rate variation = − y force coefficient derivative with yaw rate variation	0.316
$C_{Z\dot{\alpha}} = C_{Y\dot{\beta}}$	z force coefficient due to angle of attack rate variation = y force coefficient due to side slip angle rate variation	−0.441
$C_{K\delta_a}$	Rolling moment coefficient due to aileron angle variation	−0.0004
C_{Kp}	Rolling moment coefficient due to roll rate variation	−0.013
$C_{M\alpha} = -C_{N\beta}$	Pitching moment coefficient due to angle of attack variation = − Yawing moment coefficient due to side slip angle variation	−0.0347
$C_{M\delta_e} = -C_{N\delta_r}$	Pitching moment coefficient due to elevator angle variation = −Yawing moment coefficient due to rudder angle variation	−0.041
$C_{Mq} = C_{Nr}$	Pitching moment coefficient due to pitch rate variation = Yawing moment coefficient due to yaw rate variation	−0.9455
$C_{M\dot{\alpha}} = -C_{N\dot{\beta}}$	Pitching moment coefficient due to angle of attack rate variation = − Yawing moment coefficient due to side slip angle rate variation	−0.1895

research. The block diagram of the control system can be depicted schematically as Fig. 2.

Based on Fig. 2, ψ_c, θ_c and φ_c indicate the input commands of yaw, pitch and roll respectively. The error values of yaw, pitch and roll which are shown respectively as e_1, e_2 and e_3 are inputs of proportional-integral-derivative (PID) controllers and outputs of controllers are the rudder, elevator and aileron commands which are represented as δ_{rc}, δ_{ec} and δ_{ac} respectively. Commands of four actuators (δ_{1c}, δ_{2c}, δ_{3c} and δ_{4c}) are then calculated in the compensator as follows:

$$\delta_{1c} = \delta_{ac} + \delta_{ec} + \delta_{rc} \tag{20}$$

$$\delta_{2c} = \delta_{ec} - \delta_{rc} \tag{21}$$

$$\delta_{3c} = \delta_{ac} - \delta_{ec} - \delta_{rc} \tag{22}$$

$$\delta_{4c} = -\delta_{ec} + \delta_{rc} \tag{23}$$

As Fig. 1 shows, four control surfaces have a cross orientation with an angle of 45° relative to the horizon. The number of each control surface form 1 to 4 is added in a clockwise manner (North-East (1), South-East (2), South-West (3) and North-West (4)) for an observer from the behind of the vehicle. Actuators transfer the input commands to the deflection of four control surfaces (δ_1, δ_2, δ_3 and δ_4) which are inputs of the system dynamics and finally the yaw, pitch and roll angles of vehicle are the output of system dynamics. A schematic diagram of control system with PID controller for yaw channel of the AUV is depicted in Fig. 3. K_p, K_d and K_i in Fig. 3 indicate the proportional, derivative and integrator coefficients of the controller and the control law for the output of the controller of yaw channel, δ_{rc} is written as Eq. (24) [27]. It should be noted that $e_1(t)$ in Eq. (24) indicates the error of yaw angle.

$$\begin{aligned}\delta_{rc} = {} & sat\big(K_p \times e_1(t)\big) \\ & + sat\left(K_d \times lowpassed\left(\frac{\mathrm{d}\psi(t)}{\mathrm{d}t}\right)\right) \\ & + sat\big(\int [K_i \times e_1(t)]dt\big)\end{aligned} \tag{24}$$

where *sat* refer to the saturation function defined as:

$$sat(x) = \begin{cases} \operatorname{sgn}(x)x_{max}, & if\ |x| \geq x_{max} \\ x & else \end{cases}$$

As mentioned earlier, the controller of two other channels (pitch and roll) is also PID type and the control system of these two channels is similar to the yaw channel. A low pass filter is applied on the derivative part to decrease the negative effect of noise in the measurement instrument.

An AUV with an appropriate autopilot is capable of achieving a relatively high-performance. This performance is also one of the reasons of using the proper actuator which drives the control surface. Thus it may be necessary to include the dynamics of the actuator in order to have an acceptable system model. The second order linear model for the actuator is used in the present study and is presented by Eq. (25), where ζ_{Act} and ω_{Act} are the damping

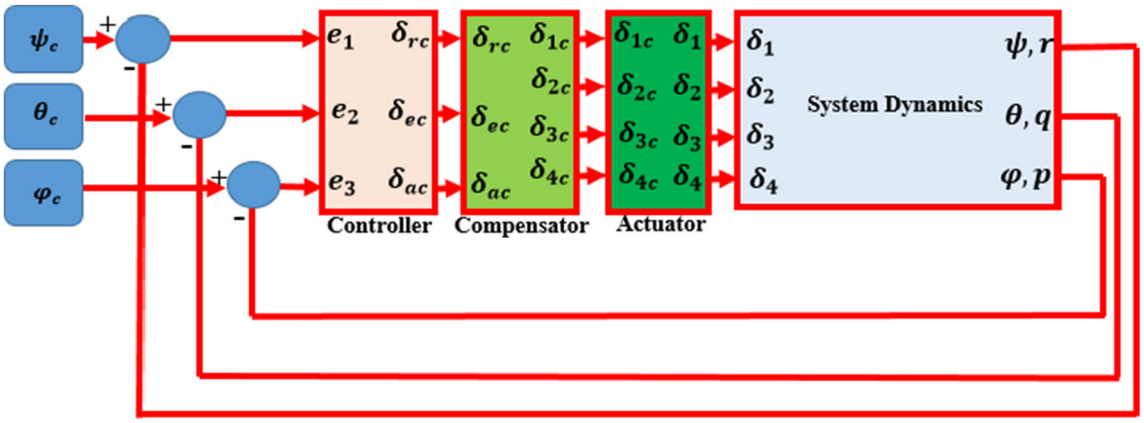

Fig. 2 Shematic of control system for the AUV

coefficient and natural frequency of the actuator respectively [28].

$$G_{actuator}(s) = \frac{\delta}{\delta_c} = \frac{\omega_{Act}^2}{s^2 + 2\zeta_{Act}\omega_{Act}s + \omega_{Act}^2}. \tag{25}$$

In Eq. (25), δ is the output of the actuator and δ_c is the input or command.

By linearization of relations and calculation of the transfer function of the vehicle from the rudder angle to the yaw angle, the transfer function can be represented as Eq. (26) which considers four dynamic coefficients.

$$G_{dynamics}(s) = \frac{\psi}{\delta_r} = \frac{Ds + E}{As^3 + Bs^2 + Cs} \tag{26}$$

where

$$A = -Y_\beta I_{zz} + muI_{zz}$$
$$B = -Y_\beta I_{zz} + N_r Y_\beta - N_\beta Y_r - mu\left(N_r - N_\beta\right)$$
$$C = N_r Y_\beta - N_\beta Y_r + muN_\beta$$
$$D = -N_\beta Y_{\delta_r} + N_{\delta_r} Y_\beta + muN_{\delta_r}$$
$$E = -N_\beta Y_{\delta_r} - N_{\delta_r} Y_\beta$$

It should be noted that all of coefficients in Eq. (26) include force and moments instead of force and moment coefficients. Therefore, $-Y_\beta$, Y_β, Y_r and Y_{δ_r} are the y force due to the side slip angle, side slip angle rate, yaw rate and rudder angle variations respectively and N_β, N_β, N_r and N_{δ_r} are the yawing moment due to the side slip angle, side slip angle rate, yaw rate and rudder angle variations respectively. As mentioned earlier the main purpose of this study is to investigate the effect of stability derivative coefficients on the performance of the control system and actuator design and therefore, the nonlinearities, cross couplings in the dynamic equations, possible delays, noises and dynamics of sensors which may significantly impact on the control system performance are not considered in the present study. The mentioned transfer function can also be presented in terms of the natural frequency and damping coefficient of the airframe as follows:

$$G_{dynamics}(s) = \frac{T_1 s + T_2}{s\left(s^2 + 2\zeta_{AF}\omega_{AF}s + \omega_{AF}^2\right)} \tag{27}$$

where $T_1 = \frac{D}{A}$, $T_2 = \frac{E}{A}$, $\omega_{AF}^2 = \frac{C}{A}$ and $\zeta_{AF} = \frac{B}{2A\omega_{AF}}$.

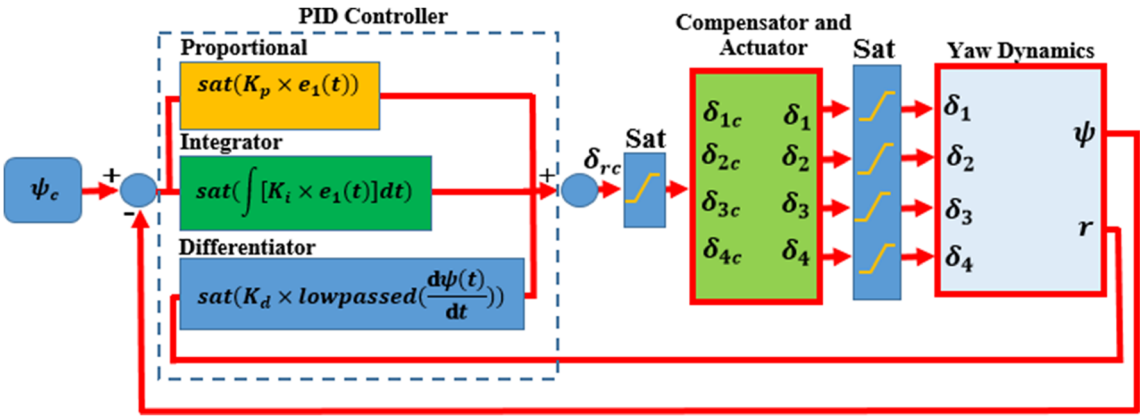

Fig. 3 Shematic of control system with PID controller for the yaw channel of the vehicle

The open-loop transfer function of the AUV by neglecting the actuator dynamics can be expressed as:

$$G_{open-loop}(s) = G_{controller}(s)G_{dynamics}(s) = \frac{K_1 s^3 + K_2 s^2 + K_3 s + K_4}{s^2(\tau s + 1)\left(s^2 + 2\zeta_{AF}\omega_{AF} s + \omega_{AF}^2\right)} \quad (28)$$

where $K_1 = K_p T_1 \tau$, $K_2 = T_1(-K_d + K_p + K_i\tau) + K_p T_2 \tau$, $K_3 = T_2(-K_d + K_p + K_i\tau) + K_i T_1$ and $K_4 = K_i T_2$.

Finally, the close-loop transfer function of the entire system can be written as the following equation:

$$G_{close-loop}(s) = \frac{G_{controller}(s)G_{system}(s)}{1 + G_{controller}(s)G_{system}(s)} \quad (29)$$

where

$$G_{controller}(s) = \frac{K_p s(\tau s + 1) + K_i(\tau s + 1) - K_d s}{s(\tau s + 1)} \quad (30)$$

$$G_{system}(s) = G_{actuator}(s)G_{dynamics}(s) \quad (31)$$

where τ is time constant parameter of the low pass filter. The bandwidth of the system is defined as the frequency at which the amplitude of output oscillations (the yaw rate here) decreases 3 dBs or almost reaches 70% of initial values of the amplitude of output oscillations. Therefore, the bandwidth of the system is calculated using the following equation:

$$\left|G_{close-loop}(j\omega_s)\right| = 0.70 \quad (32)$$

In the following section, results of the effect of dynamic stability derivatives on the actuator dynamic characteristics, airframe open loop bandwidth and airframe close loop properties in time domain and frequency domain are discussed.

4 Simulation Results and Discussion

Dynamics of the system which are represented using the hydrodynamic stability derivative coefficients are combined with the controller and actuators in the previous sections. For analysis of the control system performance, the simple and conjugate dominant poles of the closed-loop transfer function are investigated at different control gains and full hydrodynamic consideration which results in the determination of proper zones for control gains. It is tried in this section to investigate these zones in nonlinear time domain and frequency domain. Finally, the dynamic stability derivative coefficients are considered for the proper and more accurate design of the actuator.

4.1 Time Domain Analysis

In this section, at the first step, the behaviour of an AUV is compared in two cases with similar actuators by considering the dynamic stability derivatives coefficients in one case and ignoring them in another case. For this purpose, a complete six-degrees of freedom simulation in *C* software has been used. Due to the interactions of different control channels, it has tried to perform analyses in the nonlinear environment and, if possible, the transfer functions in linear environment for frequency domain analysis have been used. A 5 degree yaw command is applied to the vehicle and the results of the comparison in time domain are shown in Figs. 4, 5 and 6. As can be seen in Fig. 4, in the case of ignoring the dynamic stability derivatives coefficients, the yaw angle has a 13.9% overshoot. However, by applying the dynamic stability derivatives coefficients in the simulation, this overshoot is completely eliminated and the yaw angle has been approached to the applied command slowly. Indeed, the closed loop behaviour of the system in this case is approached to the behaviour of an under damping system.

Variation of yaw rate with time caused by the applied command is shown in Fig. 5 for two mentioned cases. As Fig. 5 shows, the maximum value of yaw rate in two cases of considering and neglecting dynamic stability derivatives coefficients are 19.0 and 24.9 deg/s respectively. Also, the results indicate that the yaw rate includes the negative values in the case of ignoring the dynamic coefficients while the yaw rate includes only positive values by applying dynamic coefficients. Therefore, according to the results, it can be resulted that the dynamic stability derivatives coefficients in the equations of motion avoid fast motions of the AUV.

In addition, Fig. 6 shows rudder control surface angle for two mentioned cases. The change of rudder angle is similar to

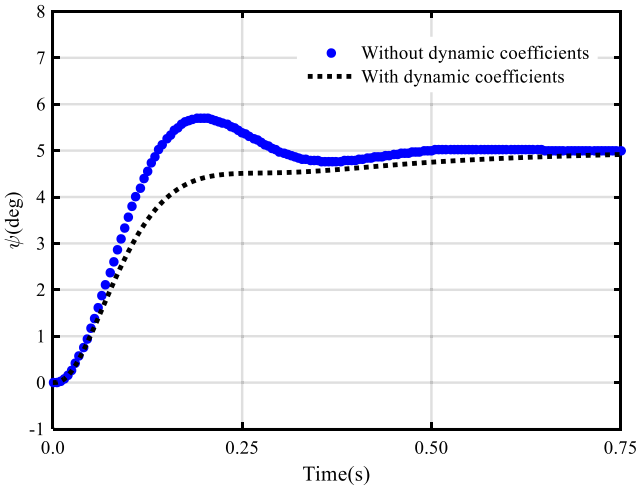

Fig. 4 Yaw angle due to 5 deg command in two cases of considering dynamic coefficients and ignoring them

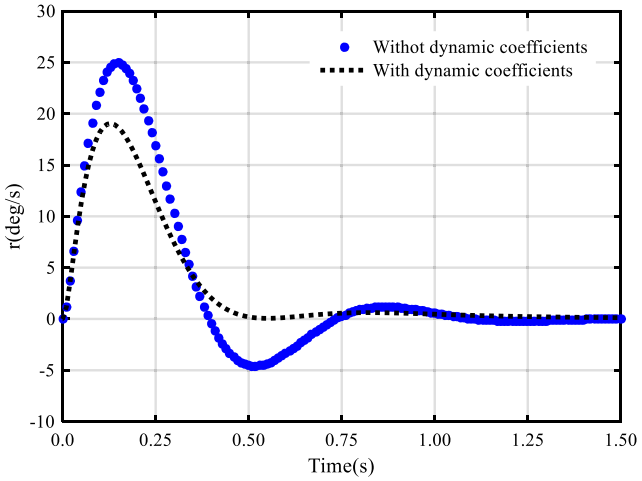

Fig. 5 Yaw rate due to 5 deg command in two cases of considering dynamic coefficients and ignoring them

the yaw rate and by considering the dynamic coefficients, the rudder angle includes the positive values only.

The bandwidth of the system will be studied in the following for two cases of open-loop and close-loop systems. In order to investigate the bandwidth of system dynamics (open loop analysis) in time domain, four different cases are considered in simulations. In the first case, no dynamic coefficient has been considered. In the second case, two dynamic coefficients C_{Yr} and C_{Nr} have been considered and the third case considers $C_{Y\dot{\beta}}$ and $C_{N\dot{\beta}}$ (added mass coefficients).In the final case all of four dynamic stability derivatives coefficients have been considered. In order to estimate the bandwidth of dynamics of the system (open-loop) in time domain, the rudder control surface angle has been chosen as a sine input with amplitude of 1 degree and variable frequency and the output of system's dynamic which is the yaw rate has been investigated. The bandwidth is defined as the frequency at which the amplitude of output oscillations (the yaw rate here) decreases 3 dBs or almost reaches 70% of initial values of amplitude of

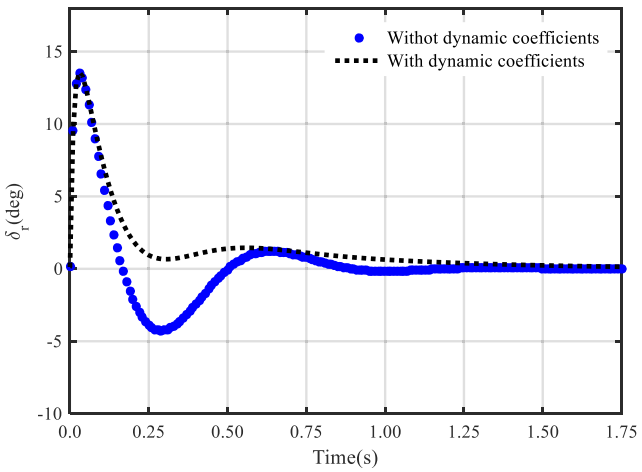

Fig 6 Rudder control surface angle due to 5 deg command in two cases of considering dynamic coefficients and ignoring them

Table 3 Results of nonlinear analysis (time domain) for open-loop system

Considered coefficients	Open-loop Bandwidth (Hz)
No dynamic coefficient	1.52
C_{Yr}, C_{Nr}	3.60
$C_{Y\dot{\beta}}$, $C_{N\dot{\beta}}$	1.35
C_{Yr}, C_{Nr}, $C_{Y\dot{\beta}}$, $C_{N\dot{\beta}}$	3.35

output oscillations. Results of the bandwidth for these four cases are shown in the Table 3. The results of open-loop analysis show that the coefficients C_{Yr} and C_{Nr} increase the bandwidth while the coefficients $C_{Y\dot{\beta}}$ and $C_{N\dot{\beta}}$ (added mass coefficients) decrease the bandwidth of the system. The effect of considering all of dynamic coefficients is increasing the bandwidth of the system by 120%.

For close-loop analysis in time domain, the yaw command has been chosen as a sine input with amplitude of 1 degree and variable frequency and the output of system which is the yaw angle has been investigated. The bandwidth in this case is also defined as the frequency at which the amplitude of output oscillations (the yaw angle here) decreases 3 dBs or almost reaches 70% of initial values of amplitude of output oscillations. The results of close-loop analysis of bandwidth are shown in the Table 4. The results of close-loop analysis for bandwidth show that the effects of dynamic coefficients become less important for the close-loop system with controller and that the dynamic coefficients have a decreasing effect on the bandwidth. The results indicate that the effect of considering dynamic coefficients in the close-loop analysis is the reduction of bandwidth by 57%. The most effects of these coefficients in the close loop are in the damping of the system which will be investigated in frequency domain analysis section. Also, the results indicate that the effect of added mass coefficients ($C_{Y\dot{\beta}}$, $C_{N\dot{\beta}}$) is negligible relative to the other two dynamic coefficients (C_{Yr}, C_{Nr}).

4.2 Frequency Domain Analysis

For analysis of the system in frequency domain, by considering the transfer function defined by Eq. (26) and introducing a sine wave as input similar to the previous cases, the bandwidth

Table 4 Results of nonlinear analysis (time domain) for close-loop system

Considered coefficients	Close-loop Bandwidth (Hz)
No dynamic coefficient	2.1
C_{Yr}, C_{Nr}	0.7
$C_{Y\dot{\beta}}$, $C_{N\dot{\beta}}$	2.0
C_{Yr}, C_{Nr}, $C_{Y\dot{\beta}}$, $C_{N\dot{\beta}}$	0.9

Table 5 Results of open-loop linear analysis (frequency domain)

Considered coefficients	Transfer function ($\frac{r}{\delta_r}$)	Natural frequency (rad/s)	Damping coefficient	Bandwidth (Hz)
No dynamic coefficient	$\frac{20.81s+71.51}{s^2+4.55s+17.81}$	4.22	0.54	1.36
C_{Yr}	$\frac{20.81s+71.51}{s^2+4.55s+25.08}$	5.01	0.45	1.88
C_{Nr}	$\frac{20.81s+71.51}{s^2+9.74s+41.43}$	6.44	0.76	2.68
C_{Yr}, C_{Nr}	$\frac{20.81s+71.51}{s^2+9.74s+48.7}$	6.98	0.70	3.22
$C_{Y\dot{\beta}}$	$\frac{20.81s+45.54}{s^2+2.9s+11.34}$	3.37	0.43	1.33
$C_{N\dot{\beta}}$	$\frac{19.68s+71.51}{s^2+5.42s+17.81}$	4.22	0.64	1.23
$C_{Y\dot{\beta}}$, $C_{N\dot{\beta}}$	$\frac{20.09s+45.54}{s^2+3.45s+11.34}$	3.37	0.51	1.26
C_{Yr}, C_{Nr}, $C_{Y\dot{\beta}}$, $C_{N\dot{\beta}}$	$\frac{20.09s+45.54}{s^2+8.87s+31.02}$	5.57	0.80	3.02

of the system dynamics (open-loop) can be calculated. Table 5 presents the results of the calculation of bandwidth for different cases of considering dynamic coefficients. Also the natural frequency and damping coefficient of the system for different cases are calculated and presented in Table 5.

The results of open-loop frequency domain analysis show that C_{Yr} and C_{Nr} coefficients increase the bandwidth of the system, while $C_{Y\dot{\beta}}$ and $C_{N\dot{\beta}}$ coefficients decrease the bandwidth of the system just like the time domain analysis (see Table 3). In the frequency domain, the effect of considering all of dynamic coefficients is increasing the bandwidth of the system by 122%. As can be shown in Table 5, the damping of the open loop system has been increased by 48% when the dynamic stability derivatives coefficients have been considered.

For close-loop analysis in frequency domain, the close-loop linearized transfer function of the system (Eq. (29)) has been considered and the bandwidth of the close-loop system has been evaluated. The results of close-loop linear analysis are presented in Table 6. Similar to the results of nonlinear analysis of close-loop system (Table 4), the results of linear analysis indicate that the effect of considering four dynamic coefficients is the reduction of bandwidth by 53%.

As can be seen in Table 6, the close-loop transfer function of the system is forth order and thus has four simple or complex conjugate poles. The dominant pole approximation can be applied to such high order systems in order to make them easier to think about. This approximation assumes that the slowest part of the system dominates the response and the faster parts of the system can be ignored. For example, the close-loop transfer function of the system with no dynamic coefficients and considering four dynamic coefficients (the first and the last rows of Table 6 respectively) have a pair of complex conjugate roots and two simple poles as shown in Table 7. It should be noted that real parts of poles determine the response speed and imaginary parts of complex conjugate roots determine the oscillatory behaviour of the system if they are dominant pole. Therefore, the magnitude of closest simple poles to the origin (a) against real parts of closest complex conjugate roots to the origin ($\zeta\omega_n$) has been compared for dominant pole determination. The ratio of $\zeta\omega_n/a$ can determine the degree of the dependence of the response to the complex conjugate pole which tends to add oscillations to the response. The higher the value of $\zeta\omega_n/a$ the further the complex conjugate pole from the origin and the closer the simple pole to the origin, which means that the effects of oscillations are less on the response of the system and the simple pole dominates the response. As can be seen in Table 7, the closest simple pole to the origin (a) is equal to −2.68 in the case of ignoring dynamic coefficients and the real part of the complex conjugate root ($\zeta\omega_n$) is equal to −4.29 for this case. Similarly, the values of a and $\zeta\omega_n$ for the case of considering four dynamic coefficients are equal to −1.64 and − 7.06 respectively. Also, the ratio of $\zeta\omega_n/a$ is equal to 1.6 and 4.3 for the cases of ignoring and considering dynamic coefficients respectively. Therefore, it can be concluded again that

Table 6 Results of close-loop linear analysis (frequency domain)

Considered coefficients	Transfer function ($\frac{\psi}{\psi_c}$)	Bandwidth (Hz)
No dynamic coefficient	$\frac{62.43s^2+6458s+21450}{s^4+104.6s^3+1160s^2+10380s+21450}$	1.70
C_{Yr}, C_{Nr}	$\frac{62.43s^2+6458s+21450}{s^4+109.7s^3+1709s^2+13470s+21450}$	0.60
$C_{Y\dot{\beta}}$, $C_{N\dot{\beta}}$	$\frac{60.27s^2+6164s+13660}{s^4+103.5s^3+1019s^2+8664s+13660}$	1.68
C_{Yr}, C_{Nr}, $C_{Y\dot{\beta}}$, $C_{N\dot{\beta}}$	$\frac{60.27s^2+6164s+13660}{s^4+108.9s^3+1580s^2+10630s+13660}$	0.79

Table 7 Close-loop transfer function poles

Considered coefficients	No dynamic coefficient	C_{Yr}, C_{Nr}, $C_{Y\beta}$, $C_{N\beta}$
Transfer function ($\frac{\psi}{\psi_c}$)	$\frac{62.43s^2+6458s+21450}{s^4+104.6s^3+1160s^2+10380s+21450}$	$\frac{60.27s^2+6164s+13660}{s^4+108.9s^3+1580s^2+10630s+13660}$
Simple poles	−2.68, −93.30	−1.64, −93.10
(a)	−2.68	−1.64
Complex conjugate poles ($\zeta\omega_n+\omega_d i$)	$-4.29+8.21i$, $-4.29-8.21i$	$-7.06+6.29i$, $-7.06-6.29i$
$\zeta\omega_n/a$	1.6	4.3
ζ	0.46	0.75

the dynamic coefficients have decreased the oscillations of the response (see Figs. 4, 5 and 6). Furthermore, the magnitudes of the damping coefficient related to complex conjugate poles are presented in Table 7 and are equal to 0.46 and 0.75 for the cases with and without considering dynamic coefficients respectively.

It should be noted that all of previous close-loop results are based on using a fixed PID controller with $K_p = 3$, $K_d = -0.3$

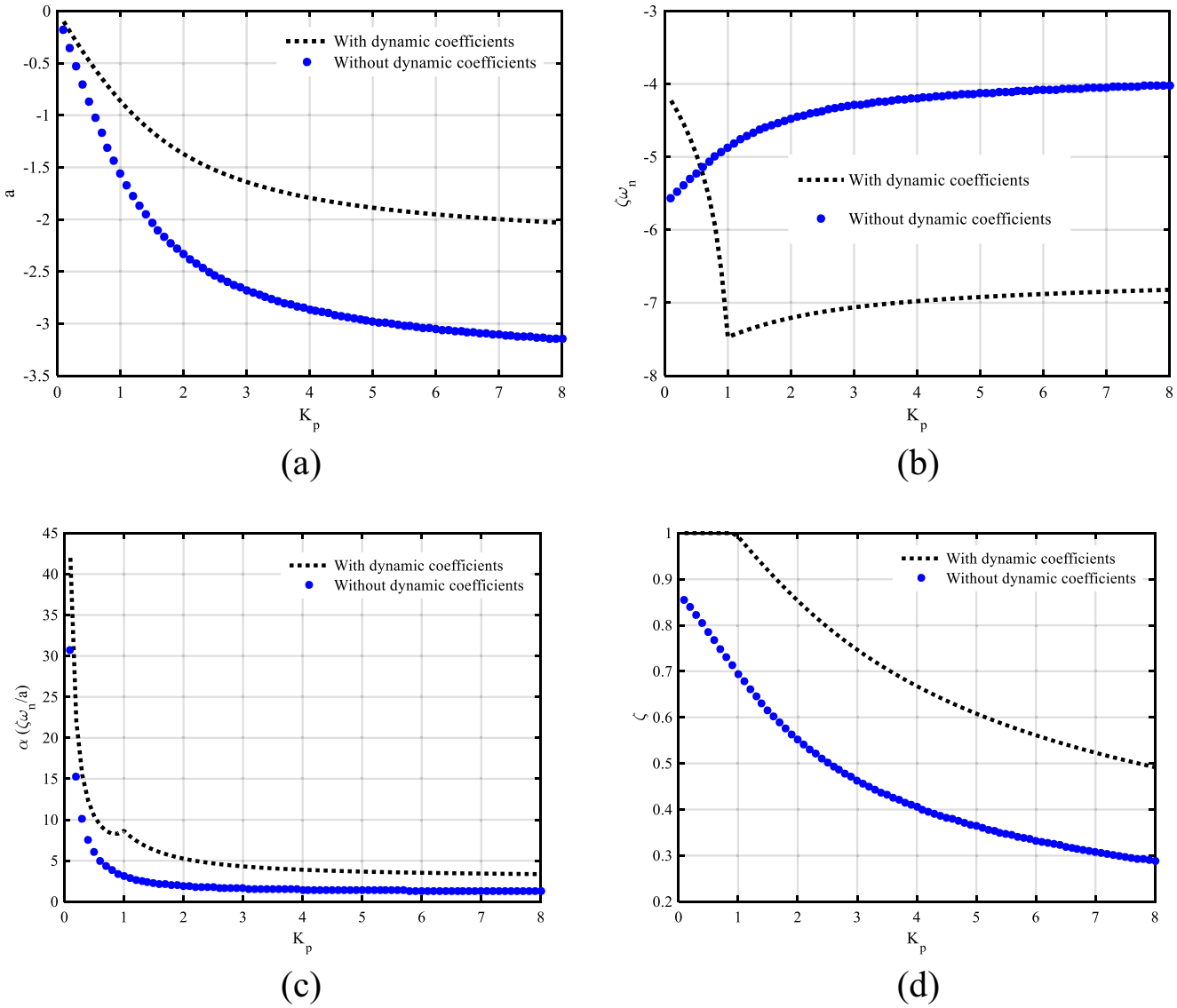

Fig. 7 Variations of **a** simple pole a, **b** real part of complex conjugate pole $\zeta\omega_n$, **c** ratio of $\zeta\omega_n/a$ and **d** variation of damping ratio of complex conjugate pole ζ with K_p

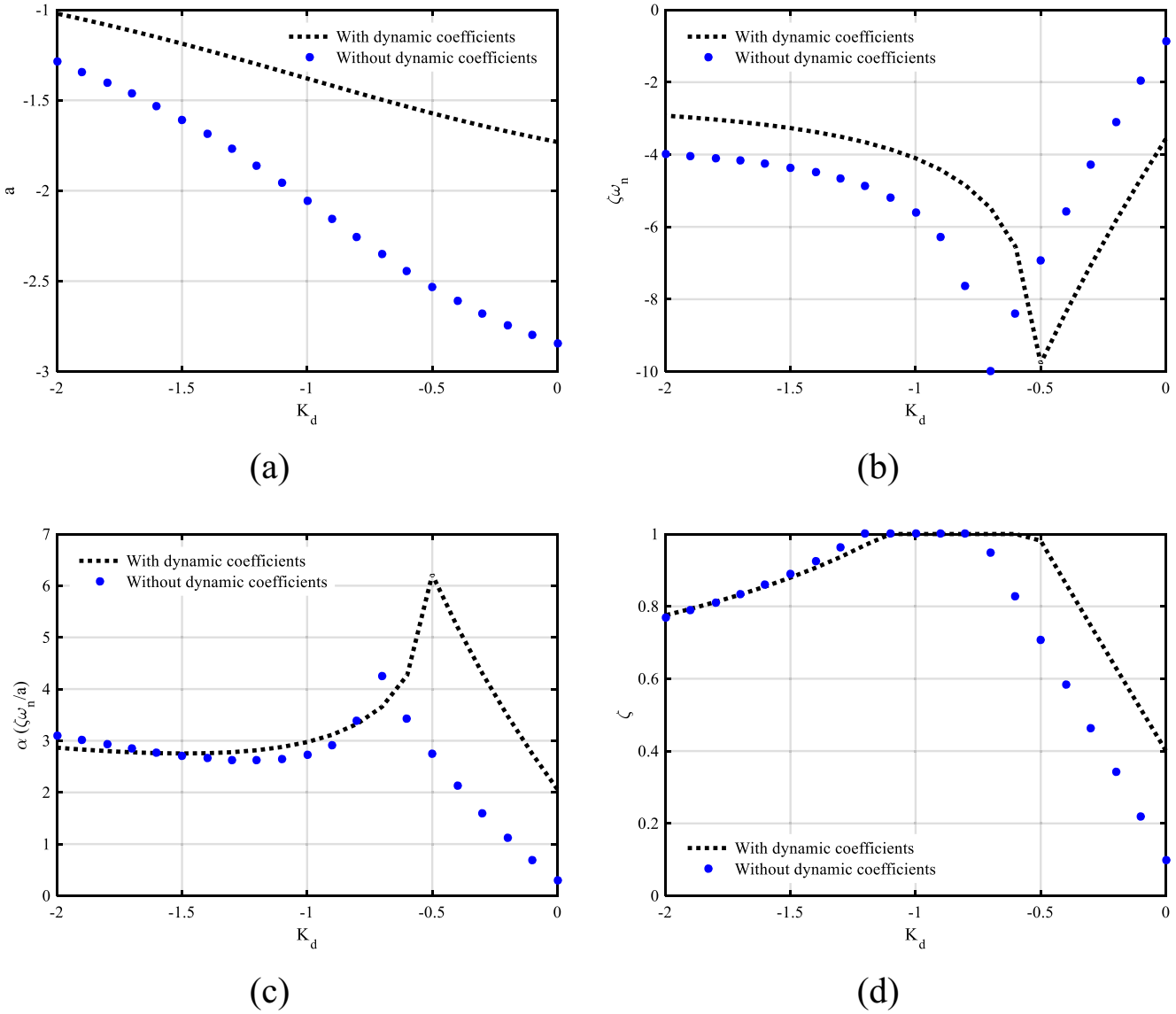

Fig. 8 Variations of **a** simple pole a, **b** real part of complex conjugate pole $\zeta\omega_n$, **c** ratio of $\zeta\omega_n/a$ and **d** variation of damping ratio of complex conjugate pole ζ with K_d

and $K_i = 0$ and ignoring the actuator dynamics. The actuator dynamics will be considered in the following section for final design of the actuators for the system. But, in order to investigate the effect of controller gains on the system performance, four results which are the magnitudes of a, $\zeta\omega_n$, $\zeta\omega_n/a$ and ζ are determined for different values of K_p, K_d and K_i and shown in Figs. 7, 8 and 9.

As discussed earliear, the higher the value of $\zeta\omega_n/a$ the further the complex conjugate pole from the origin and the closer the simple pole to the origin, which means that the effects of oscillations are less on the response of the system and the simple pole dominates the response. In other words, in order to have the best performance of the controller to decrease the oscillations of the response, the ratio of $\zeta\omega_n/a$ and the value of the damping coefficient should be as high as possible. The suggested value of the ratio is often $\zeta\omega_n/a > 5$ to ignore the effects of oscillations of complex conjugate poles based on the dominant pole approximation. As Figs. 7a and 8a show, by changing the gains K_p and K_d the simple pole of the system with dynamic stability derivatives coefficients is always closer to the origin than the simple pole of the system without considering dynamic coefficients, which means the faster response of the former system. Figure 7c shows that the ratio of $\zeta\omega_n/a$ is greater for the system with dynamic coefficients for all values of K_p, which means that the effects of oscillations are less on the response of the system with dynamic coefficients and the simple pole dominates the response. Also, the magnitudes of the damping coefficient related to the complex conjugate pole are shown in Fig. 7d and the results show that the damping coefficient is always greater

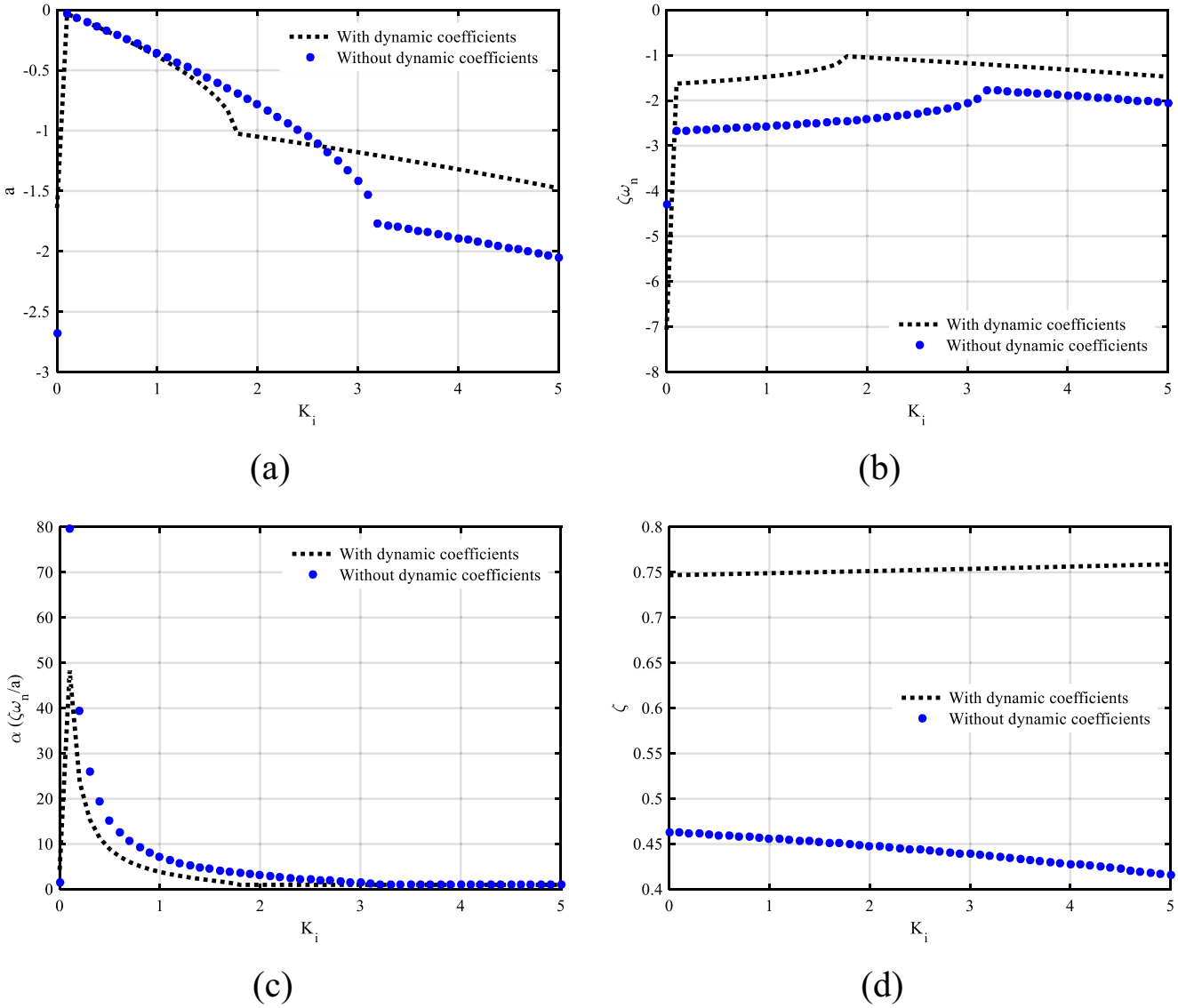

Fig. 9 Variations of **a** simple pole a, **b** real part of complex conjugate pole $\zeta\omega_n$, **c** ratio of $\zeta\omega_n/a$ and **d** variation of damping ratio of complex conjugate pole ζ with K_i

for the system with considering dynamic coefficients. Based on Fig. 8c and d, the effect of K_d on two considered systems is not significant for high magnitudes of this gain. However, the effect of gain K_d becomes more significant in smaller magnitudes and again the ratio of $\zeta\omega_n/a$ and the magnitude of damping coefficient ζ are greater for the system with considering dynamic coefficients. Figure 9 shows that the effect of integrator gain K_i is not significant on the results. It should be noted that the design of the controller is out of the scope of present study and only the effects of different gains on the system performance was investigated.

4.3 Actuator Design

The final step is to consider the dynamics of the actuator and design of proper actuator for the system in time domain and frequency domain. For this purpose, the effect of actuator natural frequency in time domain analysis is shown in Fig. 10 when the dynamic coefficients are ignored. It should be noted that the gains of the PID controller are: $K_p = 3$, $K_d = -0.3$ and $K_i = 0$. Figure 10 shows the variations of yaw angle for different natural frequencies of the actuator which are equal to 15, 20, 30 and 40 rad/s. As results show, the system is unstable at ω_{Act} of 15 rad/s. At natural frequency of 20 rad/s the system becomes stable but the maximum percentage of overshoot is equal to 61% for this case and oscillations of yaw angle around the final value is high. The maximum percentage of overshoot and oscillations of yaw angle around the final value will decrease by increasing the natural frequency of actuator. As can be seen in Fig. 10, the oscillations will disappear completely for actuator natural frequencies of 30 and 40 rad/s and the maximum percentage of overshoot for natural frequencies of 30 and 40 rad/s decreases

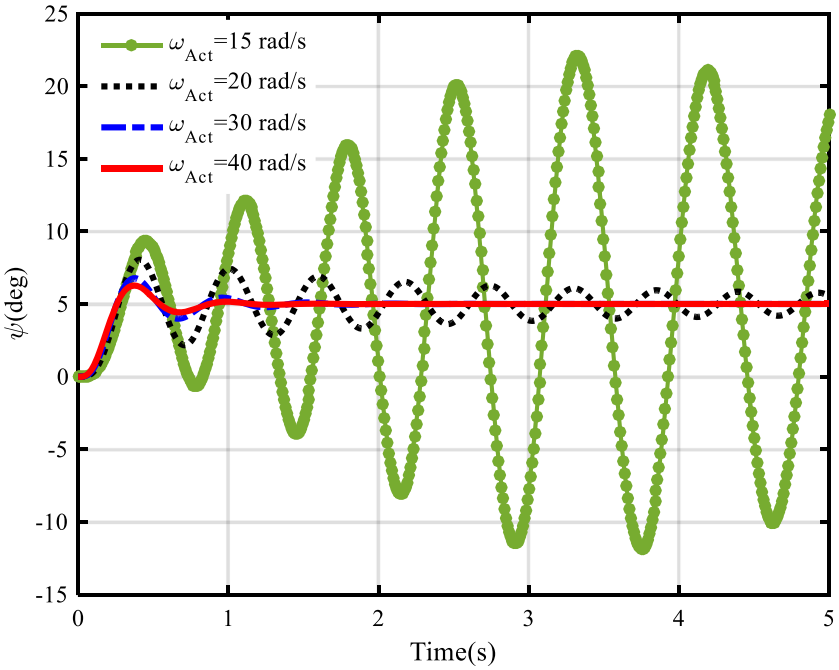

Fig. 10 Yaw angle due to 5 deg command by ignoring dynamic coefficients and in different natural frequencies of the actuator

to 35% and 25% respectively. In addition, no significant changes are seen in the yaw angle variations by increasing the natural frequency of actuator from 30 to 40 rad/s. Therefore, it can be suggested that a second order linear actuator with natural frequency of 30 rad/s and damping coefficient of 0.7 is suitable for the yaw channel of this AUV without considering the dynamic coefficients. Of course, the dynamic coefficients will be considered in the following for the proper and more accurate design of the actuator.

As mentioned, it is necessary to consider the dynamic stability derivatives coefficients in simulations in order to select the proper actuator for the AUV. The comparison in this case is done by applying dynamic coefficients and considering actuators with damping coefficient of 0.7 and natural frequencies of 5, 10, 15 and 20 rad/s. The results of actuator natural frequency effects by considering dynamic stability derivatives coefficients are shown in Fig. 11. As Fig. 11 shows, the system is unstable in natural frequency of 5 rad/s. As can be seen

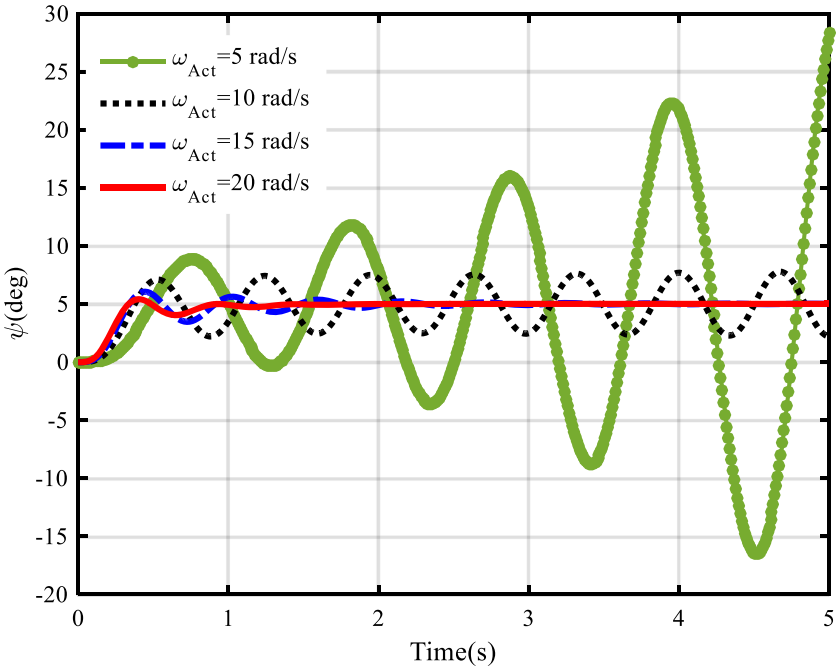

Fig. 11 Yaw angle due to 5 deg command by considering dynamic coefficients and in different natural frequencies of the actuator

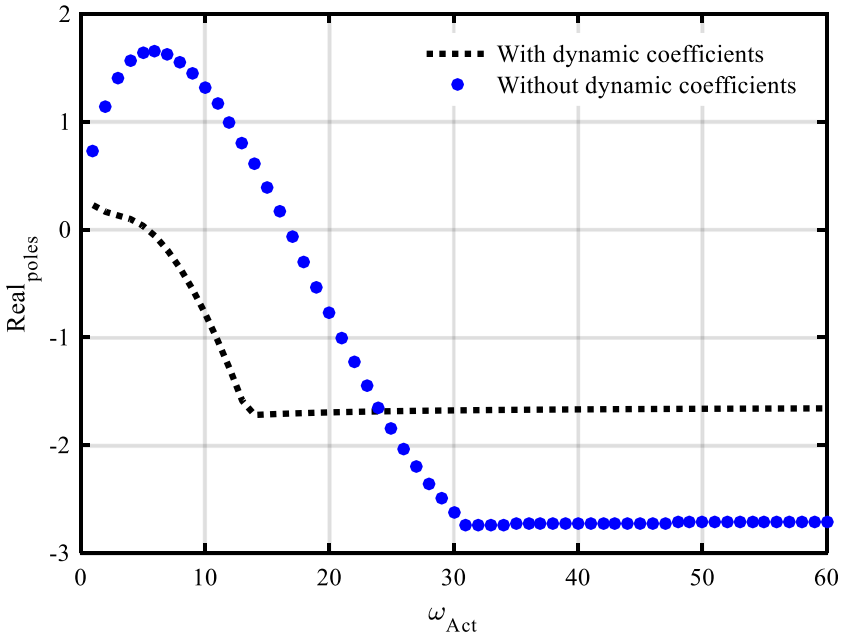

Fig. 12 Real part of the closer pole to the origin versus different natural frequencies of the actuator

in Fig. 11, the system becomes stable at ω_{Act} of 10 rad/s, but with high percentage of overshoot equal to 42% and high oscillations of yaw angle around the final value. On the other hand, by increasing the natural frequency of actuator to 15 and 20 rad/s, the system has been stabilized with the reduced maximum percentage of overshoot equal to 21% and 8% respectively. Also, the result shows that increasing the natural frequency from 15 to 20 rad/s has no significant effect on the yaw angle variations. Therefore, the comparison of results of two considered cases (ignoring and considering dynamic coefficients) indicate that by considering the dynamic stability derivatives coefficients, an actuator with a lower natural frequency (15 rad/s in comparison to 30 rad/s) can be selected for the yaw channel of the AUV.

The investigation of the effect of the actuator natural frequency can also be done in the frequency domain by considering the linearized dynamics and the close-loop transfer function of the system (see Eq. (29)). Similar to the time domain analysis a PID controller with $K_p = 3$, $K_d = -0.3$ and $K_i = 0$ is considered and an actuator with fixed damping coefficient of

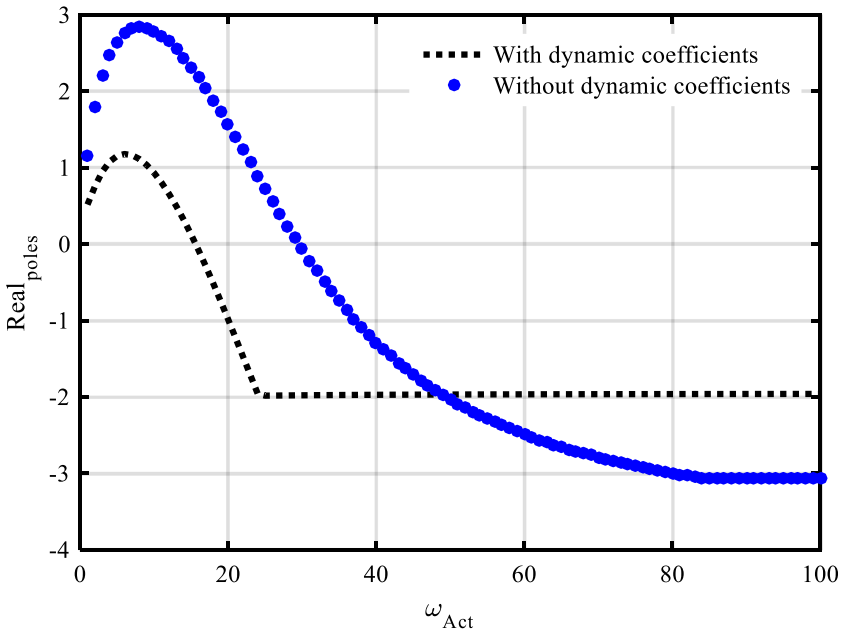

Fig. 13 Real part of the closer pole to the origin versus different natural frequencies of the actuator (PID controller with $K_p = 1.5$, $K_d = -0.3$ and $K_i = 0$)

0.7 and different natural frequencies (from 1 to 60 rad/s) has been studied. As mentioned earlier, the real part of poles determine the response speed. The real part of the closer pole to the origin (simple or complex conjugate pole) is considered in order to investigate the effect of the natural frequency of the actuator in the frequency domain. The variations of this real part $Real_{poles}$ are shown in Fig. 12 for two cases of considering and neglecting dynamic coefficients. As can be seen in Fig. 12, the graph of $Real_{poles}$ versus ω_{Act} have two different parts. The first part is at lower natural frequencies of the actuator with variations of $Real_{poles}$ which indicates that the dominant pole in this region is the complex conjugate pole and the system behaviour is oscillatory. In the second part which is at higher values of ω_{Act}, the variation of $Real_{poles}$ is almost negligible and $Real_{poles}$ has a fixed value, which indicates that the dominant pole in this region is the simple pole. In other words, after reaching to the natural frequency of the boundary between these two parts, the simple pole becomes the dominant pole of the system and the effects of oscillations of complex conjugate poles become less. Also, it should be noted that the positive values of the real part indicates the instability of the system. As Fig. 12 shows, for the system without dynamic coefficients, the magnitude of the real part of the closer pole to the origin $Real_{poles}$ is positive at ω_{Act} less than 17 rad/s and thus the system is unstable. This result is identical to the result of time domain analysis which showed that the system is unstable at ω_{Act} of 15 rad/s. For the system with dynamic coefficients, $Real_{poles}$ is positive at ω_{Act} less than 6 rad/s and thus the system is unstable at actuator natural frequencies less than 6 rad/s. This result is also identical to the result of time domain analysis which showed that the system is unstable at ω_{Act} of 5 rad/s for the system with dynamic coefficients. As mentioned, the fixed value of $Real_{poles}$ at higher natural frequencies of actuator indicates that the simple pole dominates the response and the effect of oscillations becomes less after reaching these values of ω_{Act}. Therefore, the boundary between two aforementioned parts of the graph which are almost equal to 30 and 15 rad/s for the systems without and with dynamic coefficients, can be selected approximately as the design natural frequency of the actuator (identical to the suggested values in time domain analysis).

As mentioned earlier, the gains of the PID controller are: $K_p = 3$, $K_d = -0.3$ and $K_i = 0$. However, it should be noted that the value of gains are effective on the design of the actuator for the system. As mentioned in the previous section, the design of controller is out of the scope of present study and only the effect of controller gains on the design of the actuator will be discussed. For example, the variations of $Real_{poles}$ versus ω_{Act} are shown in Fig. 13 by halving K_p (from 3 to 1.5) while keeping K_d constant (equal to −0.3). As Fig. 13 shows, halving the proportional gain results in design of an actuator with lower natural frequency than the previous case. The design natural frequencies are approximately equal to 17 and 7 rad/s for the systems without considering and with considering dynamic coefficients respectively. The results are again identical to the presented results of previous section which showed that decreasing the proportional gain K_p increases the ratio of $\zeta\omega_n/a$ and the magnitude of damping ratio ζ (see Fig. 7). Also, the variation of $Real_{poles}$ versus ω_{Act} is shown in Fig. 14 by doubling K_d (from −0.3 to −0.6) while keeping K_p constant (equal to 3). Figure 14 shows that doubling K_d has decreased the design natural frequency of the actuator from 30 to 25 rad/s for the case of ignoring dynamic coefficients and has no significant effect on the design natural

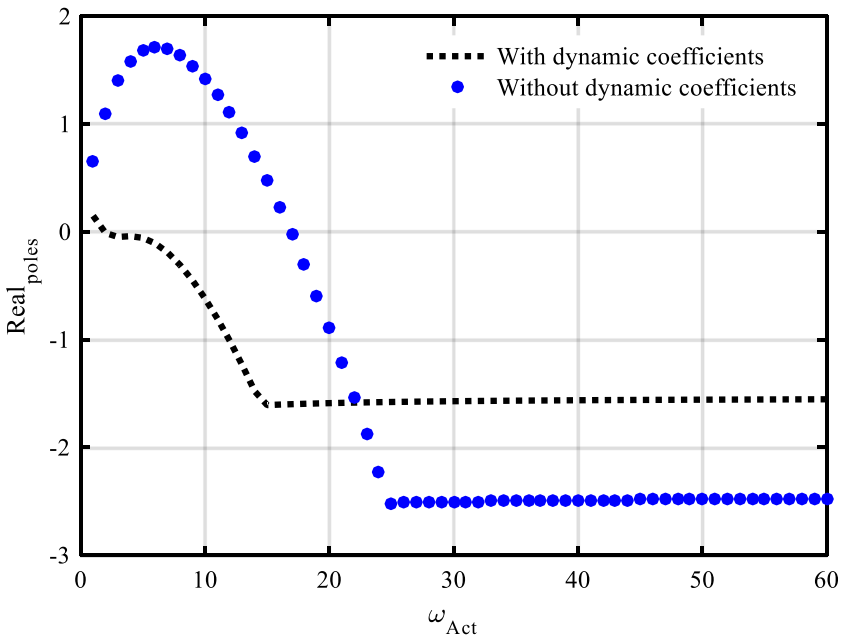

Fig. 14 Real part of the closer pole to the origin versus different natural frequencies of the actuator (PID controller with $K_p = 3$, $K_d = -0.6$ and $K_i = 0$)

frequency of actuator which is approximately equal to 15 rad/s for the case of considering dynamic coefficients. This result can also be justified using the results of previous section in Fig. 8. As can be seen in Fig. 8c and d, for the system without dynamic coefficients, doubling K_d has increased both the ratio of $\zeta\omega_n/a$ and the magnitude of damping ratio ζ which result in lower design natural frequency of the actuator (25 rad/s in comparison to 30 rad/s). On the other hand, for the system with dynamic coefficients, as Fig. 8c shows, doubling K_d has no significant effect on the ratio of $\zeta\omega_n/a$ and this ratio is equal to 4.30 and 4.27 for the gain K_d equal to −0.3 and − 0.6 respectively. Therefore, doubling K_d has no considerable effect on design natural frequency of actuator for the system with dynamic coefficients in this specific region.

5 Conclusion

In the present study, the static and dynamic stability derivatives coefficients which are calculated using Datcom computational code are modeled in the nonlinear time domain and the frequency domain to investigate their effects on the performance of an AUV and the design of proper actuators. The results show that the consideration of dynamic stability derivatives coefficients prevents fast movements of the vehicle and leads to 57% decrease in the closed loop bandwidth of the vehicle. Also, it is shown that by a full hydrodynamic consideration in modeling of the AUV, the effect of control gains and damping can be different in comparison with the cases which are not considered them. For analysis of the control system performance, the simple and conjugate dominant poles of the closed-loop transfer function are investigated at different control gains and full hydrodynamic consideration which results in the determination of proper zones for control gains. Furthermore, the effect of the natural frequency of the actuator on the performance of the AUV has been investigated and the results indicate that a lower cost actuator with lower bandwidth can be selected in the presence of dynamic stability derivatives coefficients.

References

1. Joe, H., Kim, M., Yu, S.c.: Second-order sliding-mode controller for autonomous underwater vehicle in the presence of unknown disturbances. Nonlinear Dyn. **78**(1), 183–196 (2014)
2. Randeni P, S.A.T., Forrest, A.L., Cossu, R., Leong, Z.Q., Ranmuthugala, D., Schmidt, V.: Parameter identification of a nonlinear model: replicating the motion response of an autonomous underwater vehicle for dynamic environments. Nonlinear Dyn. **91**(2), 1229–1247 (2018)
3. Ghavidel, H.F., Kalat, A.A.: Robust control for MIMO hybrid dynamical system of underwater vehicles by composite adaptive fuzzy estimation of uncertainties. Nonlinear Dyn. **89**(4), 2347–2365 (2017)
4. Xu, F., Zou, Z.-J., Yin, J.-C., Cao, J.: Identification modeling of underwater vehicles' nonlinear dynamics based on support vector machines. Ocean Eng. **67**, 68–76 (2013)
5. Conte, G., Zanoli, S.M., Scaradozzi, D., Conti, A.: Evaluation of hydrodynamics parameters of a uuv. A preliminary study. In: First International Symposium on Control, Communications and Signal Processing, pp. 545–548 (2004)
6. Morrison, A.T.I., Yoerger, D.R.: Determination of the hydrodynamic parameters of an underwater vehicle during small scale, nonuniform, 1-dimensional translation. In: MTS/IEEE Ocean. '93, pp. 11277–11282 (1993)
7. Egeskov, P., Bjerrum, A., Pascoal A.: Design, construction and hydrodynamic testing of the AUV MARIUS. Auv 94, no. August, pp. 199–207 (1994)
8. Aage, C., Wagner Smitt, L.: Hydrodynamic manoeuvrability data of a flatfish type AUV. In: Proceedings of OCEANS'94, vol. 3, pp. III/425–III/430 (1994)
9. Eng, Y., Lau, W., Low, E., Seet, G., Chin, C.: Identification of the hydrodynamics coefficients of an underwater vehicle using free decay pendulum motion. Eng. Lett. **16**(3), 326–331 (2008)
10. Suzuki, H., Sakaguchi, J., Inoue, T.: Evaluation of methods to estimate hydrodynamic force coefficients of underwater vehicle based on CFD. IFAC Proceedings Volumes. **46**(33), 1–6 (2011)
11. Praveen, P.C., Krishnankutty, P.: Study on the effect of body length on the hydrodynamic performance of an axi-symmetric underwater vehicle. Indian J Geo-Mar Sci. **42**, 1013–1022 (2013)
12. Hong, E.Y., Meng, T.K., Chitre, M.: Online system identification of the dynamics of an autonomous underwater vehicle. In: 2013 Ieee Int. Underw. Technol. Symp. (2013)
13. Nesline, F.W., Nesline, M.L.: Homing missile autopilot response sensitivity to stability derivative variations. In: Proc. 23rd Conf. Decis. Control. Las vegas, NV (1984)
14. Chwa, D., Choi, J.Y., Seo, J.H.: Compensation of actuator dynamics in nonlinear missile control. IEEE Trans. Control Syst. Technol. **12**(4), 620–626 (2004)
15. Jun-fang, F.A.N., Zhong, S.U., Qing, L.I., Si-yu, D: Design and control limitation analysis of two-loop autopilot. In: 2011 Chinese Control Decis. Conf., no. 2, pp. 3814–3818 (2011)
16. Li, B., Su, T.C.: Nonlinear heading control of an autonomous underwater vehicle with internal actuators. Ocean Eng. **125**, 103–112 (2016)
17. Sun, M., Zhang, L., Wang, Z., Chen, Z.: PID pitch attitude control for unstable flight vehicle in the presence of actuator delay: tuning and analysis. J. Frankl. Inst. **351**(12), 5523–5547 (2014)
18. Wu, N., Wu, C., Ge, T., Yang, D., Yang, R.: Pitch channel control of a REMUS AUV with input saturation and coupling disturbances. Appl. Sci. **8**(2), 253 (2018)
19. Indiveri, G., Malerba, A.: Complementary control for robots with actuator redundancy: an underwater vehicle application. Robotica. **35**(1), 206–223 (2017)
20. Lea, R.K., Allen, R., Merry, S.L.: A comparative study of control techniques for an underwater flight vehicle. Int. J. Syst. Sci. **30**(9), 947–964 (1999)
21. Hsu, S.P., Liu, T.S.: Modifications of control loop to improve the depth response of autonomous underwater vehicles. Math. Probl. Eng. (2014)
22. Fossen, T.I.: Handbook of Marine Craft Hydrodynamics and Motion Control. Wiley, Chichester (2011)
23. Banazadeh, A., Seif, M.S., Khodaei, M.J., Rezaie, M.: Identification of the equivalent linear dynamics and controller design for an unmanned underwater vehicle. Ocean Eng. **139**, 152–168 (2017)

24. Ansari, U., Bajodah, A.H., Alam, S.: Generalized dynamic inversion based attitude control of autonomous underwater vehicles. IFAC-PapersOnLine. **49**(23), 582–589 (2016)
25. Watson, K.P.: Prediction of fin loads on missiles in incompressible flow. In: 6th Applied Aerodynamics Conference, pp. 228–238 (1998)
26. Gan, W., Zhu, D., Xu, W., Sun, B.: Survey of trajectory tracking control of autonomous underwater vehicles. J. Mar. Sci. Technol. **25**(6), 722–731 (2017)
27. Upadhyay, V., et al.: Design and motion control of autonomous underwater vehicle, Amogh. In: Underw. Technol. 2015 IEEE, p. 9 (2015)
28. McLean, D.: Automatic Flight Control Systems. Prentice Hall International, London (1990)

Mojtaba Mirzaei is assistant professor in the Hydro-Aeronautical Research Center (HARC), Shiraz University, Shiraz, Iran. He received his MSc. and Ph.D. from Shiraz University in 2009, 2014 respectively, and in 2014 joined the Hydro-Aeronautical Research Center in Shiraz University. He received the B.Sc. degrees in Mechanical Engineering in 2006 from Isfahan University of Technology, Isfahan, Iran. His research interests include aerospace robot control, underwater robot control, and fault-tolerant control.

Hossein Taghvaei received his B.Sc. and MSc. degrees in Mechanical Engineering and Energy Conversion and now is a Ph.D. candidate of Mechanical Engineering, Energy Conversion at School of Mechanical Engineering at the Shiraz University (since September 2014). He is a member of the council of university gifted students at Shiraz University since 2008 and a member of National Elite Foundation of Iran since 2014. His research interest includes renewable energy, solar desalination, ground source heat pumps, and autonomous underwater vehicles. Currently he studies different aspects of autonomous underwater vehicles such as water entry and control.